Supercapacitor Sizing for Fast Power Dips in a Hybrid Supercapacitor—PEM Fuel Cell System

Giovanni Dotelli, Roberto Ferrero, *Member, IEEE*, Paola Gallo Stampino, Saverio Latorrata, and Sergio Toscani, *Member, IEEE*

***Abstract*— Polymer electrolyte membrane fuel cell (PEM FC) operation is likely to be characterized by voltage dips on timescales shorter than 1 s, arising from temporary flooding of gas channels or porous layers, particularly when the FC is operated at high humidity levels. If supercapacitors are employed in hybrid systems, they can make up for the temporary lack of energy produced by the FC. However, the steep slopes of the voltage dips affect the energy that can be actually delivered by the supercapacitor because of its series impedance, and this should be taken into account when sizing it. This paper presents a simplified approach for sizing the supercapacitor, based on some observed peculiar features of the FC dips, which allow a simple but accurate model for the evaluation of the supercapacitor response to such dips. The validity of such an approach is supported by simulation and experimental results performed on a single PEM FC and on a supercapacitor.**

***Index Terms*— Analytical models, fuel cells (FCs), power dip, power transients, supercapacitor response, supercapacitor sizing, supercapacitors.**

I. Introduction

THE use of fuel cells (FCs) and particularly polymer electrolyte membrane (PEM) FCs for power generation has been widely studied in the last decades, and many applications are gradually appearing on the market [1], [2]. However, the complex FC behavior characterized by the interplay of several electrochemical processes has not been completely understood yet, and control systems are often unable to guarantee optimal operating conditions, particularly when sophisticated systems cannot be employed because of their high cost.

As a result, unexpected voltage variations are likely to appear during the FC operation, on different timescales depending on the causes of such variations. In particular, unpredictable and deep voltage dips may occur when water temporarily clogs the gas channels or porous layers, preventing the gas from reaching the active layers where the chemical reaction takes place [3], [4]. Such cell flooding may happen when water builds up in the cell as a consequence of nonoptimal water management or unexpected sudden changes in the operating conditions, and it represents one of the most important causes of performance degradation and voltage instability at high currents.

FCs can be employed both in grid-connected [5] and in stand-alone systems, whose typical examples are FC vehicles [6]. Concerning stand-alone applications, it is worth noting that FCs are usually integrated with other auxiliary energy sources or storage systems in so-called hybrid systems. The main reason for this is related to the slow dynamics of FCs, which are not able to effectively deal with fast load changes. In a hybrid system, the FC cooperates with other sources (such as batteries or supercapacitors) thanks to power converters supervised by a master control system [7], [8]. In this way, a fast dynamic response of the whole system is achieved, while the FC operates in almost stationary conditions even in the case of sudden load changes, such as strong accelerations and regenerative braking in powertrain applications.

The vast majority of papers on this topic available in the literature are focused on control strategies aimed at dealing with the load energy demand [9]–[11]. However, as stated before, in some cases the power produced by the FCs may exhibit sudden dips that have to be covered by the other energy sources in hybrid systems. On the other hand, to the authors' best knowledge, little attention has been paid to the ability of such sources to compensate for the temporary lack of energy produced by the FC when the above-mentioned voltage dips occur.

Even for a supercapacitor, which typically shows better dynamic behavior than that of conventional batteries, the short timescale (under 1 s) of the fast dips may become critical, as it affects the energy that can be actually delivered, significantly decreasing it with respect to the nominal specifications. This should be taken into account for a correct choice of the supercapacitor size in the design of the hybrid power system. Significant differences between the supercapacitor response and an ideal capacitor response were confirmed by preliminary results reported in [12], based on a measured FC voltage dip, an experimentally identified supercapacitor model, and a simulation of the hybrid FC-supercapacitor system.

In this paper, the above-mentioned simulation results are validated by experimental tests. Moreover, a simplified analytical approach is presented, suitable for sizing the supercapacitor when it is employed to cover the fast energy dips produced by the FC. This method is based on peculiar features of the FC energy dips, investigated through a more comprehensive

Manuscript received November 9, 2015; revised February 9, 2016; accepted March 17, 2016. Date of publication April 20, 2016; date of current version September 12, 2016. The Associate Editor coordinating the review process was Dr. Carlo Muscas.

G. Dotelli, P. Gallo Stampino, and S. Latorrata are with the Department of Chemistry, Materials, and Chemical Engineering G. Natta, Politecnico di Milano, Milan 20133, Italy (e-mail: giovanni.dotelli@polimi.it; paola.gallo@polimi.it; saverio.latorrata@polimi.it).

R. Ferrero is with the Department of Electrical Engineering and Electronics, University of Liverpool, Liverpool L69 3GJ, U.K. (e-mail: roberto.ferrero@liverpool.ac.uk).

S. Toscani is with the Dipartimento di Elettronica, Informazione e Bioingegneria, Politecnico di Milano, Milan 20133, Italy (e-mail: sergio.toscani@polimi.it).

experimental analysis, which allow a simple but accurate modeling of the supercapacitor response to such dips.

II. Fuel Cell Fast Energy Dips

A. Water Management and Instabilities

Water management is one of the most critical issues for proper operation of a PEM FC. Indeed, the cell membrane needs to be well humidified to keep ohmic losses low and avoid damages, but on the other hand, water buildup within the cell worsens gas transport through the gas channels and the porous gas diffusion and catalyst layers, thus reducing the efficiency and possibly damaging the cell. The control of the optimal humidity level within the cell is made particularly difficult by the water production at the cathode, whose rate depends on the generated current, and by the complex water transport processes across the membrane [3], [13], [14]. Therefore, at least sporadically, nonoptimal humidity levels are likely to occur during the FC operation.

Both the opposite failure modes associated with water management, namely, membrane dehydration and cell flooding, may lead to some instabilities in the FC voltage, though with very different features. In the first case, when the membrane is not fully hydrated, small random variations in the membrane humidity give rise to corresponding variations in the membrane ohmic resistance, which in turn produce continuous oscillations of the FC voltage. Being driven by humidity variations, such voltage instability occurs on long timescales (tens or hundreds of seconds) [15]. On the other hand, water buildup within the cell due to an excessive amount of water may lead to a sudden clog of gas paths with consequent gas starvation. This produces an immediate and often very significant voltage drop on a timescale shorter than 1 s, which then rapidly vanishes as soon as the water clog is removed by the pressure increase originated by the clog itself, thus appearing as a fast transient in the voltage waveform [3], [4].

Although many diagnostic approaches have been studied to detect drying and flooding occurrences [16]–[19], also based on low-cost instrumentation suitable for commercial applications [20]–[22], the FC control may still be unable to avoid the appearance of some voltage dips because of their sudden and unpredictable nature.

B. Experimental Results on a Single Cell

A typical example of the above-mentioned FC voltage dips is shown in Fig. 1, which was measured on a single PEM FC operated at constant current (21.9 A). The cell is composed of commercial materials, with Nafion 212 as electrolyte (23-cm^2 active area), and it is fed with humidified hydrogen and air at the anode and cathode, respectively. Being the current kept constant by an electronic load, the cell power is proportional to the voltage, and the energy dip can be calculated from the difference between the power during the transient and the constant power produced before it. The result is also shown in Fig. 1. If the load connected to the FC requires a constant power, a secondary power source or energy storage system should make up for such an energy dip. In more detail, in the example of Fig. 1, the voltage decrease transient lasts for about 0.1 s, so the secondary power source must be able to promptly deliver the required energy to the load.

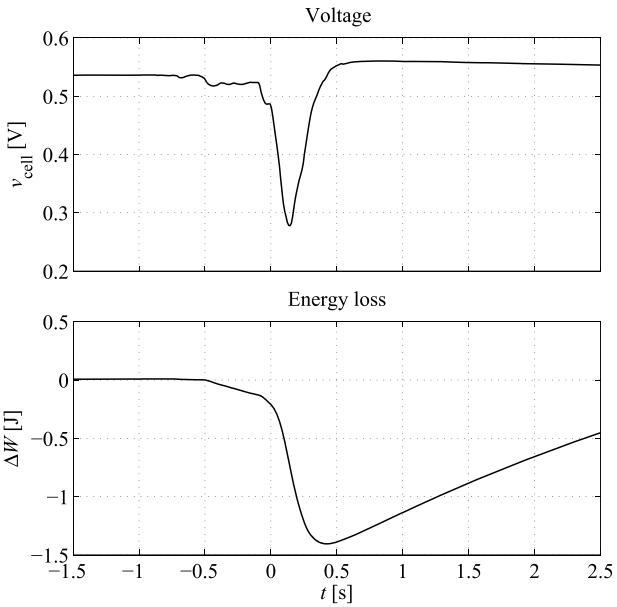

Fig. 1. Typical voltage dip (top) and corresponding energy dip (bottom), measured on a single PEM FC operated at constant current (21.9 A).

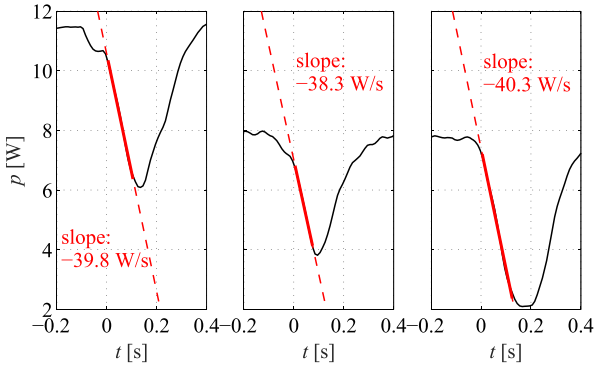

Fig. 2. Power dips measured in different operating conditions; a linear fit of the decreasing part of the transient is superimposed to each power waveform and its slope value is provided.

It should be noted that the energy dip shown in Fig. 1 is just an example, and different dips can appear in different operating conditions and even in nominally identical conditions, because of the essentially unpredictable nature of the phenomena producing the water clog. However, some common features can be observed in power dips with different amplitudes and measured in different operating conditions. Fig. 2 shows the power waveform corresponding to the same dip reported in Fig. 1, compared with other two dips measured at lower current and characterized by different amplitudes. For all of them, the decreasing part of the transient is almost linear, except for the very first instants. A linear fit of the power transient is superimposed to each waveform, confirming the linear behavior with good accuracy. Moreover, the slopes of such linear fits are almost constant for all dips (the values are reported in Fig. 2), and they appear to be independent of the FC operating conditions and the dip amplitude. It is also worth noting that the three dips were measured with different

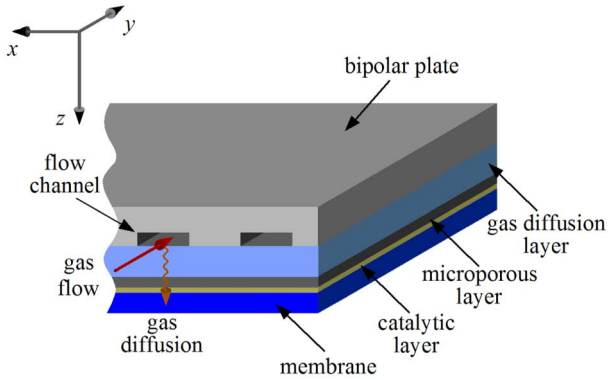

Fig. 3. Cross view of the flow fields, GDL, and MEA.

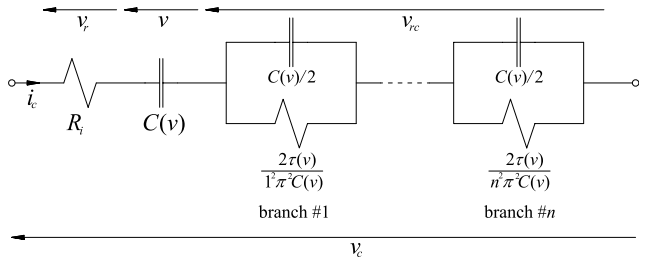

Fig. 4. Equivalent circuit of the supercapacitor derived from (1); an infinite number of RC branches should be theoretically considered.

membranes (though with the same nominal specification), so the constant value of the power slope appears to be a general feature related only to the cell design and the type of material.

A simple interpretation of this property can be formulated according to the following description of local processes occurring within the cell. Fuel and oxidant are fed to the cell through the flow fields of bipolar plates; then, to reach the anodic or cathodic active layers (electrodes), they have to diffuse orthogonally through the gas diffusion layer (GDL), which is the component located between the plate and the membrane electrode assembly (MEA). The GDL is a two-layer material: a macroporous carbon cloth is in contact with the bipolar plate and the gas channels, and a microporous layer (MPL) is in contact with the MEA. In the present setup the active catalytic layer is directly coated onto the MPL, creating the so-called gas diffusion electrode. For clarity, a cross view of the system is schematically represented in Fig. 3, where gas fed through the flow field channels (in the xy plane) reaches the catalytic layer by diffusing into the GDL (along the z-direction).

Electrochemical reactions occur on the active sites of the catalytic layers (electrodes) that are in contact with the membrane. In normal operating conditions, the current can be reasonably assumed to be uniformly distributed on the active area, but when the above-mentioned water clog causing the fast energy dip occurs, it entails a local shortage of chemical reactants and a consequent sharp decrease in current density, which must be compensated by a sharp current density increase in the other regions of the active area, being the total current kept constant by the electronic load. This in turn leads to a proportional variation of the rate of reactant consumption in a control volume around the active layer; assuming a step increase in local current density, the reactant concentration near the active layer would decrease linearly with time, and this would bring about a linear change of the exchange current density and eventually a similar decrease in the cell potential [23]. The mathematical derivation of the linear voltage variation based on an integral (macroscopic) model is reported in the Appendix.

Under these hypotheses, the rate of cell power decrease would depend only on intrinsic properties of the system, except for local current density, namely, reaction constant, pore volume, and effective diffusion coefficient. This could explain why in different operating conditions the same slope is observed, which can therefore be effectively employed for sizing the required supercapacitor to cover the FC energy dip.

It should be finally noted that in a real commercial application, an FC stack composed of several cells would be employed instead of a single cell. In this case, temporary flooding transients such as those described above would be much more complex and they could propagate to other cells in the stack in different ways depending on the stack design and on the operating conditions. Nevertheless, it is reasonable to assume that single cells in the stack could be affected by fast energy dips similar to those shown above, and that such dips could occur simultaneously on several cells. Moreover, the water clog causing the energy dip in one cell could move to the adjacent cell after it is removed from the first one, thus causing a sequence of energy dips in several cells in a short time. From the supercapacitor point of view, they would be similar to a single bigger dip if the time interval is short enough with respect to the system dynamics, so that the supercapacitor is not properly recharged. Therefore, for the sake of simplicity, this paper focuses on the sizing of a supercapacitor to cover the energy dip produced by a single cell, but the results could be conceptually extended also to the case of a supercapacitor bank sized for an FC stack.

III. Supercapacitor Model

Several models have been proposed in the literature to describe the behavior of supercapacitors, which can be applied to study different phenomena ranging from fast transients to slow self-discharge. In the frequency range from tens of millihertz to hundreds of hertz, neglecting inductive phenomena, the following frequency domain model can be employed [24], [25]:

$$Z(j\omega, v) = R_i + \frac{\tau(v)\coth\left(\sqrt{j\omega\tau(v)}\right)}{C(v)\sqrt{j\omega\tau(v)}} \tag{1}$$

where R_i represents the limit resistance at infinite frequency, $C(v)$ is the dc capacitance value, which in turn depends on the voltage v on this equivalent capacitor, and $\tau(v)$ is a voltage-dependent time constant. The voltage v is assumed to change slowly with respect to the angular frequency ω.

This model can be represented in terms of an equivalent electrical circuit, as shown in Fig. 4, with a theoretically infinite number of series-connected RC branches, although a

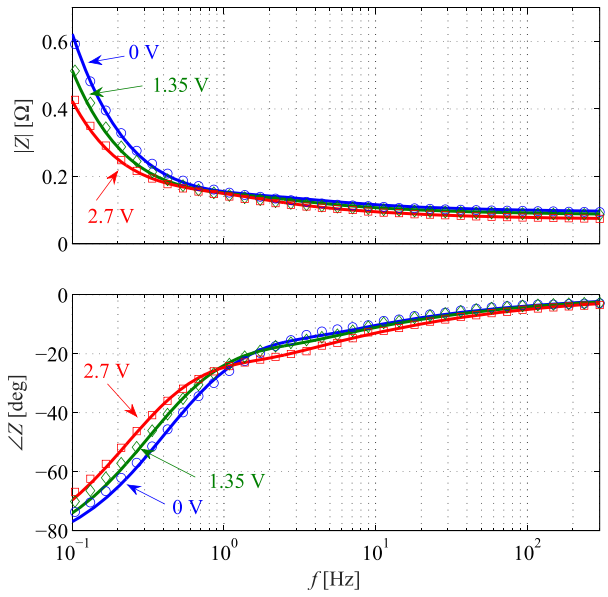

Fig. 5. Measured impedance spectra of the 3.3-F supercapacitor at three dc voltage values, namely, 0 V (blue circles), 1.35 V (green diamonds), and 2.7 V (red squares) and their fit (solid lines) according to model (1).

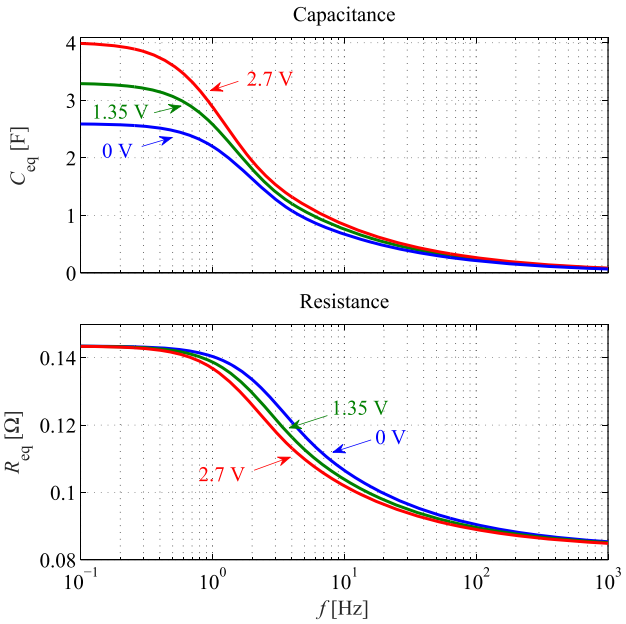

Fig. 6. Equivalent capacitance (top) and resistance (bottom) of the 3.3-F supercapacitor, according to (1) with the parameters in Table I, plotted for three dc voltage values, namely, 0 V (blue), 1.35 V (green), and 2.7 V (red).

TABLE I
IDENTIFIED PARAMETERS OF THE 3.3-F SUPERCAPACITOR

C_0	k	R_i	$R_{\rm dc}$
2.59 F	0.52 F/V	83 mΩ	143 mΩ

small number of them (four/five) are usually enough to obtain a sufficiently accurate model.

The dependence of C and τ on voltage can be assumed to be linear with a good approximation

$$\begin{aligned} C(v) &= C_0 + kv \\ \tau(v) &= \tau_0 + k_\tau v \end{aligned} \tag{2}$$

and the following relationship can be derived from (1):

$$\tau(v) = 3C(v)(R_{\rm dc} - R_i) \tag{3}$$

having defined $R_{\rm dc}$ as the low-frequency limit of the real part of (1) [25]. Thus, the model is completely defined by four parameters, namely, C_0, k, R_i, and $R_{\rm dc}$, which can be experimentally identified.

Experimental tests were performed on a 3.3-F supercapacitor (Maxwell BCAP0003) with a 2.7 V nominal voltage. The supercapacitor impedance was measured by an EIS-capable potentiostat (BioLogic SP-150) in the frequency range from 0.1 to 300 Hz, at three different dc voltage values (namely, 0, 1.35, and 2.7 V) and the results are reported in Fig. 5. The experimental data were fitted by the model (1) in a least-squares sense, and the fitted curves are also reported in Fig. 5, showing good agreement with the measured values in the selected frequency range. The identified model parameters are reported in Table I.

To better illustrate the supercapacitor behavior at different frequencies, Fig. 6 shows the equivalent capacitance $C_{\rm eq}$ and resistance $R_{\rm eq}$ at the three considered dc voltage values, calculated according to the identified model parameters assuming to represent the supercapacitor by means of an RC series model

$$Z(j\omega, v) = R_{\rm eq}(v) + \frac{1}{j\omega C_{\rm eq}(v)}. \tag{4}$$

Fig. 6 clearly shows that the capacitance starts falling before 1 Hz, and this can be explained by the porous structure of the electrodes and the limited electrolyte ion mobility [26]. Therefore, this frequency dependence is expected to affect the supercapacitor response to the fast FC power dips.

It should be noted that supercapacitors with different nominal capacitances and/or voltages are characterized by a similar frequency dependence of the equivalent capacitance and resistance. In particular, supercapacitors of the same family, having the same rated voltage, can be assumed to be composed of the same elementary cells, while the only difference is the number of such cells connected in parallel. This means that the parameters reported in Table I are approximately directly or inversely proportional to the nominal capacitance value. Therefore, the time constant $\tau(v)$ does not change significantly, according to (3).

Even if different supercapacitor families are considered, their behavior in frequency remains similar to the supercapacitor chosen here, so the analysis carried out in this paper can be considered to have a general validity.

IV. HYBRID FC-SUPERCAPACITOR SYSTEM

A. Simulation Results

Having defined the supercapacitor model, its response to a power dip when it is employed in a hybrid FC-supercapacitor system can be investigated. A schematic of a typical configuration [11], which is considered here as a case study, is shown in Fig. 7. The FC dc/dc converter controls the FC current, as it is usually done in many applications [9], so that the FC can be

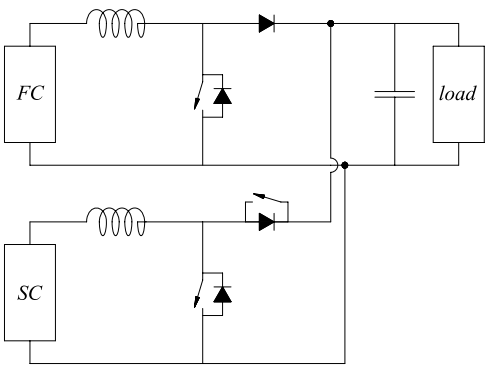

Fig. 7. Schematic of the considered hybrid FC-supercapacitor system.

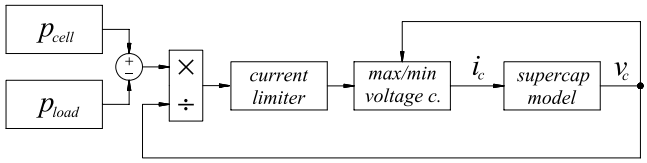

Fig. 8. Block diagram representing the simulated operation of the supercapacitor in the hybrid system.

assumed to be operated at constant current on short timescales, such as those characterizing the considered transient. On the other hand, the supercapacitor dc/dc converter is controlled in such a way to ensure that the dc bus voltage remains constant as far as possible.

Therefore, when a fast dip similar to those shown in Figs. 1 and 2 occurs, the supercapacitor will supply the required current to make up for the lack of power produced by the FC. This ideal operation (converter losses have been neglected) can be simulated in MATLAB/Simulink according to the block diagram shown in Fig. 8. For the sake of simplicity, the supercapacitor is assumed here to be initially charged at its nominal voltage when the energy dip occurs.

The simulated supercapacitor voltage (v_c) in response to the energy dip shown in Fig. 1 is reported in Fig. 9, where the different contributions to the total voltage are also highlighted, according to the equivalent circuit in Fig. 4. It clearly appears that there is a significant difference between the voltage v on the equivalent capacitor C, representing the energy storage element in the equivalent circuit, and the actual voltage v_c on the whole supercapacitor. Such a difference is due to the voltage drops on the equivalent resistor R_i and on the equivalent RC branches. In particular, the former is dominant in the first stage of the transient, when the supercapacitor voltage is decreasing.

It is interesting to note that, while the voltage v is monotonically decreasing during the whole duration of the energy dip (as expected, because the supercapacitor is supplying the required energy to cover such a dip), the overall supercapacitor voltage v_c reaches its minimum value approximately when the power requested to the supercapacitor reaches its maximum value. This happens because the voltage drop in the series elements in the equivalent circuit is significantly higher than the voltage decrease in the storage element due to the

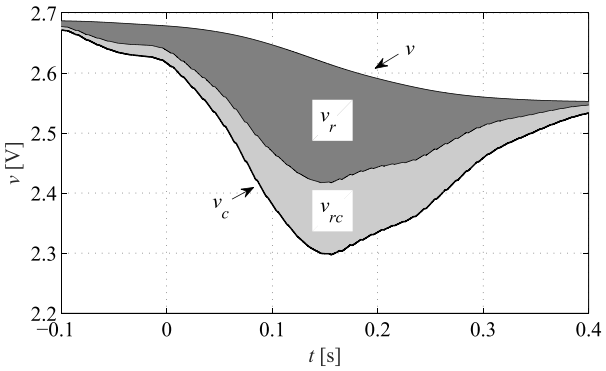

Fig. 9. Simulated supercapacitor voltage (v_c) in response to the FC energy dip shown in Fig. 1 and its three contributions v, v_r, and v_{rc} according to the equivalent circuit in Fig. 4.

supercapacitor discharge. In other words, the supercapacitor voltage decrease during the considered fast transient is much greater than what could be expected according to energetic considerations alone. This implies that the supercapacitor is not able to deliver the whole stored energy on short timescales, such as those considered here.

This phenomenon has to be considered when sizing the supercapacitor for the hybrid system, as it strongly affects the actual available energy to make up for the sudden lack of power produced by the FC when temporary flooding occurs. Its impact has to be carefully evaluated, especially for applications where steep load changes are not expected, and therefore the dynamic response of the energy storage system has not been considered in the design. Furthermore, this issue may become even more critical when the temporary flooding occurs while the supercapacitor is already generating power to deal with a fast load transient, according to the hybrid system control strategy.

B. Experimental Results

The simulation results are validated by experimental tests carried out by applying the three power waveforms shown in Fig. 2 to the supercapacitor through an electronic load. Both the supercapacitor voltage and the current were measured during each transient, and they are reported in Fig. 10, compared with the simulated waveforms. The good agreement between measurement and simulation results confirms the validity of the supercapacitor model for the purposes of this paper, particularly as far as the current waveform is concerned.

It is worth noting that for the two deepest energy dips, the maximum current generated by the supercapacitor is over 2.4 A, while the maximum acceptable current according to the supercapacitor specification is 1.9 A. On the other hand, the energy supplied by the supercapacitor is less than 2 J for all the transients, while the nominal energy of the supercapacitor (derived from its nominal voltage and capacitance) is 12 J. Thus, it appears that these fast FC power dips are more critical for the supercapacitor in terms of maximum current capability than energy storage capacity, and the supercapacitor design to cover such dips must therefore be based on the former and not on the latter.

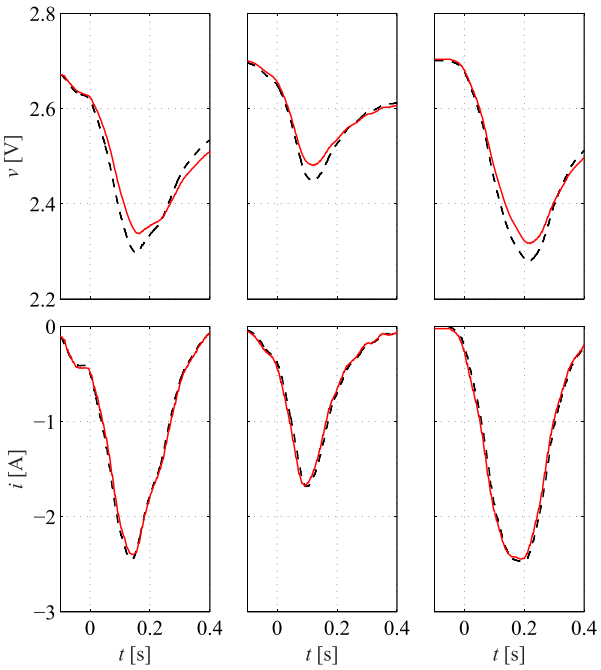

Fig. 10. Simulated (black dashed lines) and measured (red solid lines) supercapacitor voltage (top) and current (bottom) waveforms in response to the three power dips shown in Fig. 2.

In general, evaluating the maximum current requested to the supercapacitor to make up for an FC energy dip requires either a software simulation or an experimental test, because of the complex frequency- and voltage-dependent supercapacitor model and the dip waveform. The results shown above confirm that both approaches lead to very similar results, practically indistinguishable, but they are often not suitable for the first design stage as they require experimental tests either to directly measure the maximum current or to identify the model parameters necessary for the simulation (not enough information is usually included in the specification provided by the manufacturer).

To address this issue, in the following section a simplified analytical model is presented, suitable for a first rough estimate of the maximum supercapacitor current, with a reasonable accuracy but without the need for experimental tests.

V. Simplified Supercapacitor Sizing Method

The results reported in the previous sections show two important features that can be used to formulate a simplified supercapacitor sizing method. First, the maximum current generated by the supercapacitor is approximately reached at the deepest point of the FC power dip, and therefore it can be evaluated by considering only the decreasing part of the dip transient. Second, such decreasing transient can be modeled as a power ramp with constant slope, with very good approximation.

As a consequence, the maximum supercapacitor current can be estimated from the supercapacitor response to a power ramp, and its value will only depend on the ramp duration (or equivalently the ramp amplitude), being the ramp slope practically constant. Given a maximum power dip amplitude for the supercapacitor design, the maximum current will therefore be calculated and the supercapacitor will be sized accordingly.

TABLE II
Estimated, Simulated, and Measured Maximum Currents

	Test 1	Test 2	Test 3
Simplified estimate	-2.24 A	-1.62 A	-2.25 A
Simulation result	-2.44 A	-1.68 A	-2.47 A
Measurement result	-2.40 A	-1.68 A	-2.45 A

Even with a power waveform as simple as a ramp, an accurate evaluation of the supercapacitor response would require a software simulation, but the supercapacitor model can be greatly simplified for a first rough estimate, thus allowing an analytical solution. Indeed, according to Fig. 9, the main contribution to the supercapacitor voltage drop arises from the equivalent resistance R_i, therefore, the supercapacitor equivalent circuit can be reduced to an ideal capacitor C connected to the series resistor R_i. This assumption leads to the following expression for the supercapacitor voltage (with the sign convention used in Fig. 4):

$$v_c = v + v_r = v + R_i i_c \tag{5}$$

and consequently for the supercapacitor power

$$p_c = v_c i_c = v i_c + R_i i_c^2. \tag{6}$$

For the whole duration of the transient, the voltage v on the storage element can be assumed to be constant and equal to the nominal voltage $V_n = 2.7$ V, because the decrease in the stored energy is negligible compared with the nominal energy. Thus, assuming that the maximum supercapacitor current $i_{c,\max}$ corresponds to the peak power p_{peak} at the end of the power ramp, the former can be derived as

$$i_{c,\max} = \frac{-V_n + \sqrt{V_n^2 + 4R_i p_{\text{peak}}}}{2R_i}. \tag{7}$$

The estimates of $i_{c,\max}$ thus obtained are reported in Table II, compared with the simulated and measured values shown in Fig. 10. It can be seen that the relative difference between the estimated and measured (or simulated) values is less than 10% for all the three considered cases, and thus the method is accurate enough to be employed for a first sizing of the supercapacitor.

It is worth noting that the value of R_i used in (7) is the value reported in Table I, experimentally identified from the supercapacitor frequency response. This value was used here for a meaningful comparison between the estimated maximum current and simulation and measurement results. However, an estimate (or maximum value) of the equivalent series resistance is usually included in the supercapacitor specification provided by the manufacturer, therefore the method presented here does not require experimental tests carried out on the supercapacitor, and it can be effectively employed in the first design stage of a hybrid FC-supercapacitor system.

VI. Conclusion

The behavior of a hybrid power system composed of a PEM FC and a supercapacitor was investigated, in response to fast power dips that are likely to occur on the FC when it is operated at high humidity levels. Experimental tests carried out on a single PEM FC revealed peculiar features of the power dips, which allowed the formulation of a simplified analytical model to estimate the supercapacitor response to such dips, particularly in terms of the maximum current requested to the supercapacitor, which is the limiting factor in the supercapacitor sizing for this application.

In order to validate the model and justify its assumptions, the supercapacitor response to the FC energy dips was experimentally measured, and also simulated in MATLAB/Simulink based on an experimentally identified supercapacitor model. The series impedance of the supercapacitor was shown to significantly affect the delivered energy on the short timescales of the dips, causing a voltage decrease in the supercapacitor much higher than what is expected according to energy considerations alone.

The maximum current values estimated according to the simplified analytical model differed from the measured and simulated values by less than 10%, thus confirming that the proposed method can be effectively employed for a first rough sizing of the supercapacitor for the considered application.

Appendix

The physical interpretation of the fast energy dip reported in Section II-B was based on a local description of the processes occurring within the cell. From an external point of view, an integral (macroscopic) model can be formulated in terms of the overall current produced by the cell. The current is kept constant by the electronic load, which means that the average current density is also constant, as the cell active catalytic area does not change during the transient (no macroscopic degradation of the electrodes occurs).

The current–voltage relationship in dc conditions (polarization curve) can be expressed as follows:

$$V_{\text{cell}} = E^0 - R_{\text{ohm}} I_{\text{cell}} - \frac{RT}{\alpha F} \ln \frac{I_{\text{cell}}}{I_0} - \frac{RT}{nF} \ln \frac{I_L}{I_L - I_{\text{cell}}} \tag{8}$$

where E^0 is the theoretical potential, R_{ohm} is the ohmic resistance, R is the universal gas constant, T is the cell temperature, F is Faraday's constant, α is the transfer coefficient, n is the number of electrons involved in the reaction (i.e., 2), I_0 is the exchange current, and I_L is the limit current.

As a first approximation, the voltage variation during the fast energy dip can be modeled by calculating the derivative of (8) with respect to time. In (8), I_{cell} is constant because it is imposed by the load and E^0, R_{ohm}, and I_L are not expected to change during the considered transient. Thus, the only time-dependent variable is the exchange current I_0, defined as the rate at which electrochemical reactions proceed at the equilibrium [27]. Therefore, the voltage derivative results in

$$\frac{dv_{\text{cell}}}{dt} = \frac{d}{dt}\left(-\frac{RT}{\alpha F} \ln \frac{I_{\text{cell}}}{i_0}\right) = \frac{RT}{\alpha F i_0} \frac{di_0}{dt} \tag{9}$$

where i_0 is now written in lowercase, since it is time-variant.

The exchange current is in turn proportional to the concentration c of reactant, according to the following expression [27]:

$$i_0(t) = AnFkc(t) \tag{10}$$

being A the cell active area and k the chemical reaction constant. The latter can be expressed as a function of the Gibbs free energy ΔG of the electrochemical reaction and the temperature [23]

$$k = \frac{k_B T}{h} \exp\left(-\frac{\Delta G}{RT}\right) \tag{11}$$

being k_B and h Boltzmann's constant and Planck's constant, respectively. Therefore, k can be assumed to be constant here.

The concentration in the diffusive path of the gas toward the catalytic layer decreases because of the water droplets blocking the porous materials of the device. Assuming that only a 1-D (along z) variation of concentration takes place (orthogonal to gas stream in the flow field), the gas molar flow N can be written, from Fick's first law, as follows [28]:

$$N = -D^{\text{eff}} \frac{dc}{dz} = -\frac{D^{\text{eff}}}{u_z} \frac{dc}{dt} \tag{12}$$

being D^{eff} the mean diffusion coefficient of gas within the pores of the GDL and u_z the average linear gas velocity (assumed to be constant). Since N is directly proportional to I_{cell} (according to Faraday's law), the derivative of the concentration with respect to time is constant

$$\frac{dc}{dt} = -\frac{I_{\text{cell}} u_z}{AnF D^{\text{eff}}}. \tag{13}$$

Therefore, according to (9) and (10), the derivative of the cell voltage, and therefore the derivative of the cell power, with respect to time are also constant. The measured values of this derivative are also compatible with typical values of all the parameters appearing in the above equations, as they can be found in the literature.

References

[1] F. Barbir, *PEM Fuel Cells: Theory and Practice*, 2nd ed. Amsterdam, The Netherlands: Elsevier, 2013.

[2] Y. Wang, K. S. Chen, J. Mishler, S. C. Cho, and X. C. Adroher, "A review of polymer electrolyte membrane fuel cells: Technology, applications, and needs on fundamental research," *Appl. Energy*, vol. 88, no. 4, pp. 981–1007, 2011.

[3] H. Li *et al.*, "A review of water flooding issues in the proton exchange membrane fuel cell," *J. Power Sour.*, vol. 178, no. 1, pp. 103–117, 2008.

[4] G. Dotelli, R. Ferrero, P. G. Stampino, S. Latorrata, and S. Toscani, "Combining electrical and pressure measurements for early flooding detection in a PEM fuel cell," *IEEE Trans. Instrum. Meas.*, vol. 65, no. 5, pp. 1007–1014, May 2016.

[5] S. K. Mazumder, R. K. Burra, R. Huang, M. Tahir, and K. Acharya, "A universal grid-connected fuel-cell inverter for residential application," *IEEE Trans. Ind. Electron.*, vol. 57, no. 10, pp. 3431–3447, Oct. 2010.

[6] U. R. Prasanna, P. Xuewei, A. K. Rathore, and K. Rajashekara, "Propulsion system architecture and power conditioning topologies for fuel cell vehicles," *IEEE Trans. Ind. Appl.*, vol. 51, no. 1, pp. 640–650, Jan./Feb. 2015.

[7] H. Ramírez-Murillo, C. Restrepo, J. Calvente, A. Romero, and R. Giral, "Energy management of a fuel-cell serial–parallel hybrid system," *IEEE Trans. Ind. Electron.*, vol. 62, no. 8, pp. 5227–5235, Aug. 2015.

[8] J. P. Torreglosa, P. García, L. M. Fernández, and F. Jurado, "Predictive control for the energy management of a fuel-cell–battery–supercapacitor tramway," *IEEE Trans. Ind. Informat.*, vol. 10, no. 1, pp. 276–285, Feb. 2014.

[9] P. Thounthong, S. Raël, and B. Davat, "Energy management of fuel cell/battery/supercapacitor hybrid power source for vehicle applications," *J. Power Sour.*, vol. 193, no. 1, pp. 376–385, 2009.

[10] T. Azib, O. Bethoux, G. Remy, C. Marchand, and E. Berthelot, "An innovative control strategy of a single converter for hybrid fuel cell/supercapacitor power source," *IEEE Trans. Ind. Electron.*, vol. 57, no. 12, pp. 4024–4031, Dec. 2010.

[11] A. S. Samosir and A. H. M. Yatim, "Implementation of dynamic evolution control of bidirectional DC–DC converter for interfacing ultracapacitor energy storage to fuel-cell system," *IEEE Trans. Ind. Electron.*, vol. 57, no. 10, pp. 3468–3473, Oct. 2010.

[12] R. Ferrero, S. Toscani, G. Dotelli, P. G. Stampino, and S. Latorrata, "Response of a hybrid supercapacitor—PEM fuel cell system to fast fuel cell energy dips," in *Proc. IEEE Int. Workshop AMPS*, Aachen, Germany, Sep. 2015, pp. 67–71.

[13] W. Dai *et al.*, "A review on water balance in the membrane electrode assembly of proton exchange membrane fuel cells," *Int. J. Hydrogen Energy*, vol. 34, no. 23, pp. 9461–9478, 2009.

[14] N. Yousfi-Steiner, P. Moçotéguy, D. Candusso, D. Hissel, A. Hernandez, and A. Aslanides, "A review on PEM voltage degradation associated with water management: Impacts, influent factors and characterization," *J. Power Sour.*, vol. 183, no. 1, pp. 260–274, 2008.

[15] G. Dotelli, R. Ferrero, P. G. Stampino, and S. Latorrata, "Analysis and compensation of PEM fuel cell instabilities in low-frequency EIS measurements," *IEEE Trans. Instrum. Meas.*, vol. 63, no. 7, pp. 1693–1700, Jul. 2014.

[16] J.-M. Le Canut, R. M. Abouatallah, and D. A. Harrington, "Detection of membrane drying, fuel cell flooding, and anode catalyst poisoning on PEMFC stacks by electrochemical impedance spectroscopy," *J. Electrochem. Soc.*, vol. 153, no. 5, pp. A857–A864, 2006.

[17] W. Mérida, D. A. Harrington, J. M. Le Canut, and G. McLean, "Characterisation of proton exchange membrane fuel cell (PEMFC) failures via electrochemical impedance spectroscopy," *J. Power Sour.*, vol. 161, no. 1, pp. 264–274, 2006.

[18] N. Fouquet, C. Doulet, C. Nouillant, G. Dauphin-Tanguy, and B. Ould-Bouamama, "Model based PEM fuel cell state-of-health monitoring via ac impedance measurements," *J. Power Sour.*, vol. 159, no. 2, pp. 905–913, 2006.

[19] F. Barbir, H. Gorgun, and X. Wang, "Relationship between pressure drop and cell resistance as a diagnostic tool for PEM fuel cells," *J. Power Sour.*, vol. 141, no. 1, pp. 96–101, 2005.

[20] G. Dotelli, R. Ferrero, P. G. Stampino, S. Latorrata, and S. Toscani, "Diagnosis of PEM fuel cell drying and flooding based on power converter ripple," *IEEE Trans. Instrum. Meas.*, vol. 63, no. 10, pp. 2341–2348, Oct. 2014.

[21] G. Dotelli, R. Ferrero, P. G. Stampino, S. Latorrata, and S. Toscani, "PEM fuel cell drying and flooding diagnosis with signals injected by a power converter," *IEEE Trans. Instrum. Meas.*, vol. 64, no. 8, pp. 2064–2071, Aug. 2015.

[22] G. Dotelli, R. Ferrero, P. G. Stampino, S. Latorrata, and S. Toscani, "Low-cost PEM fuel cell diagnosis based on power converter ripple with hysteresis control," *IEEE Trans. Instrum. Meas.*, vol. 64, no. 11, pp. 2900–2907, Nov. 2015.

[23] V. S. Bagotsky, *Fundamentals of Electrochemistry*, 2nd ed. Hoboken, NJ, USA: Wiley, 2006.

[24] S. Buller, E. Karden, D. Kok, and R. W. De Doncker, "Modeling the dynamic behavior of supercapacitors using impedance spectroscopy," *IEEE Trans. Ind. Appl.*, vol. 38, no. 6, pp. 1622–1626, Nov./Dec. 2000.

[25] V. Musolino, L. Piegari, and E. Tironi, "New full-frequency-range supercapacitor model with easy identification procedure," *IEEE Trans. Ind. Electron.*, vol. 60, no. 1, pp. 112–120, Jan. 2013.

[26] B. E. Conway, *Electrochemical Supercapacitors: Scientific Fundamentals and Technological Applications*. New York, NY, USA: Springer, 1999.

[27] E. Chen, "Thermodynamics and electrochemical kinetics," in *Fuel Cell Technology Handbook*, G. Hoogers, Ed. Boca Raton, FL, USA: CRC Press, 2003.

[28] L. You and H. Liu, "A parametric study of the cathode catalyst layer of PEM fuel cells using a pseudo-homogeneous model," *Int. J. Hydrogen Energy*, vol. 26, no. 9, pp. 991–999, 2001.